A Cascadia Slab Model from Receiver Functions

Wasja Bloch[1], Michael Bostock[1], Pascal Audet[2]

This is a non-peer reviewed preprint submitted to *EarthArXiv.*

[1]The University of British Columbia, Vancouver, Canada
[2]University of Ottawa, Ottawa, Canda

Key Points:

- We model Cascadia subduction stratigraphy as three dipping horizons
- Slab morphology is controlled by crystalline terrane backstops
- A near-ubiquitous $\sim$ 2–10 km thick ultra-low velocity zone in tremor zone correlates with E-layer

Corresponding author: Wasja Bloch, `wbloch@eoas.ubc.ca`

Abstract

We map the characteristic signature of the subducting Juan de Fuca and Gorda plates along the entire Cascadia forearc from northern Vancouver Island, Canada to Cape Mendocino in northern California, USA, using teleseismic receiver functions. The subducting oceanic crustal complex, possibly including subcreted material, is characterized by three horizons capable of generating mode-converted waves: a negative velocity contrast at the top of a low velocity zone underlain by two horizons representing positive contrasts. The amplitude of the conversions varies likely due to differences in composition and/or fluid content. We analyzed the slab signature for 298 long-running land seismic stations, estimated the depth of the three interfaces through inverse modeling and fitted regularized spline surfaces through the station control points to construct a margin-wide, double-layered slab model. Crystalline terranes that act as the static backstop form the major structural barrier that controls slab morphology. Where the backstop recedes landward beneath Olympic Peninsula and Cape Mendocino, the slab subducts sub-horizontally, while the seaward-protruding and thickened Siletz terrane beneath central Oregon causes steepening of the slab. A tight bend in slab morphology south of Olympic Peninsula coincides with the location of recurring large intermediate depth earthquakes. The top-to-Moho thickness of the slab generally exceeds the thickness of the oceanic crust by 2-12 km, suggesting thickening of the slab or underplating of slab material to the overriding North American plate.

Plain Language Summary

The tectonic Juan de Fuca plate, that underlays the easternmost North Pacific Ocean off-shore Vancouver Island, Washington, Oregon and northern California, is being pushed beneath the North American continent by plate tectonics. On its way deep into the Earth the plate deforms. In this study, we analyze seismograms of distant earthquakes which were recorded within the study area. Through specialized signal and data processing we work out information about the location, orientation and properties of the down-going oceanic plate beneath the continent. The data show that the plate protrudes shallowly dipping under the continent beneath Olympic Peninsula (Washington) and Cape Mendocino (California) while it dips down more steeply under central Oregon and Vancouver Island (British Columbia). This configuration suggests that Siletzia, an old and rigid basalt plateau that forms the central part of the study area, controls the shape of the down-going plate. Furthermore, the oceanic plate appears to significantly thicken at depth, which may indicate that parts of it accumulate at the bottom of the continent. These results are important to better understand how plates subduct, and may help to infer the location of the deeper part of the rupture area of a future big earthquake.

1 Introduction

The boundary between the down-going oceanic and overriding continental plates in subduction zones is the locus of major seismic moment release in great earthquakes and enigmatic slow earthquakes. Knowledge about its location and orientation is key to understanding seismogenesis, tsunamigenesis, and geodynamic processes taking place in subduction zones. During subduction, the down-going slab is subjected to mechanical and chemical alterations, including flexure, shearing, increases in temperature and pressure, metamorphism, fluid generation and redistribution, metasomatism, and other complex geodynamical processes. All of these factors are expected to influence the slab's mechanical behaviour.

In the Cascadia subduction zone, the Juan de Fuca plate (JdF) subducts beneath the North American plate at velocities that vary between 42 mm yr^{-1} at its northern end near the Nootka Fault Zone, to 36 mm yr^{-1} at its southern end, near the Blanco Fracture Zone, with an azimuth of ∼N56°E. To the south, the Gorda micro-plate subducts at 33 mm yr^{-1} with an azimuth of N52°E (**?**). The Explorer plate to the north does not subduct, but more likely underthrusts the North American Plate beneath northern Vancouver Island (**???**). To the north and south, the subduction system transforms into the right-lateral Queen Charlotte and San Andreas Faults, respectively (Fig. 1).

Immediately landward of the deformation front, the subduction interface can be identified in high-frequency reflection seismic sections along the entire Cascadia margin (e.g., **????????**). In places, the structural décollement is located within the lower part of the sedimentary blanket, implying sediment subduction (**????**).

Farther downdip, the JdF has been identified below the Salish Sea on marine seismic sounding transects through the Juan de Fuca Strait and Georgia Strait. At about 20 km depth, the sharp <2 km thick reflector that marks the top of the slab widens into an up to 10 km wide reflection band, the so-called E-layer (e.g., **??**), that extends to depths of at least ∼50 km (**?**). A similarly thick reflective zone has been identified atop the subducting JdF at 35-40 km depth beneath central Oregon (**??**). It has been argued that the E-layer represents the transition into a wider shear zone that creeps aseismically and hosts episodic tremor and slip (ETS, see e.g. **??**).

At lower frequencies (∼1 Hz), the subduction zone stratigraphy can be characterized using teleseismic P-wave receiver function data (e.g., **????????**). A recent study employing receiver functions, local tomography and seismic reflection data in southern Vancouver Island suggests that the oceanic crust resides below the E-layer (**?**) and that at least part of the E-layer comprises an ultra-low S-wave velocity zone (ULVZ), with V_P/V_S in the order of 2–3 (**??**). In local seismic tomograms, the slab stratigraphy oftentimes appears smeared into a single layer with moderately elevated V_P/V_S in the order of 1.8–2.0, consistent with basaltic or gabbroic lithologies with some contribution of fluid-filled pores. Interpretation of the oceanic Moho in tomographic models is less ambiguous, where it appears as a strong negative V_P/V_S gradient to values below 1.7 that mark the oceanic mantle below (**????**).

An initial margin-wide map of the top of the JdF was constructed from a mixed dataset of earthquake hypocenters, active source seismic profiles, receiver functions and local earthquake tomograms with the aim to model interseismic strain accumulation in the overriding plate (**?**). With increasing data availability over time and a better understanding of subduction processes, the initial model has been updated and extended in space using additional constraints from seafloor magnetic anomalies, deeper seismicity and diffraction of strong earthquake first arrivals (**?**) and later from relocated earthquake hypocenters and electrical conductivity profiles (**??**). Other slab models are based purely on receiver functions (**??**). Despite a broad agreement in recovered slab depths to within ∼10 km, considerable differences exist across these models. These differences are associated with data uncertainties, the fact that the slab models are based on different data types, and with ambiguities in the interpretation of proxies for what constitutes the "slab top" (**?**).

Here, we construct a margin-wide slab model that honors an oceanic crustal stratigraphy including the possibility of subcreted material that may consist of up to two layers. Our model is based on the observation that receiver function images of the slab exhibit characteristic successions of positively and negatively polarized conversions that can be explained by interfering forward- and back-scattered seismic wave modes originating at three interfaces. We map these interfaces continuously along dip from the coast to the forearc lowlands (Salish Sea, Willamette Valley) and along strike from Brooks Peninsula on northern Vancouver Island, Canada, to Cape Mendocino, USA (Fig. 1). Our results demonstrate how the overall slab morphology is controlled by the location of the static backstop. A subduction stratigraphy that is generally thicker than the incoming

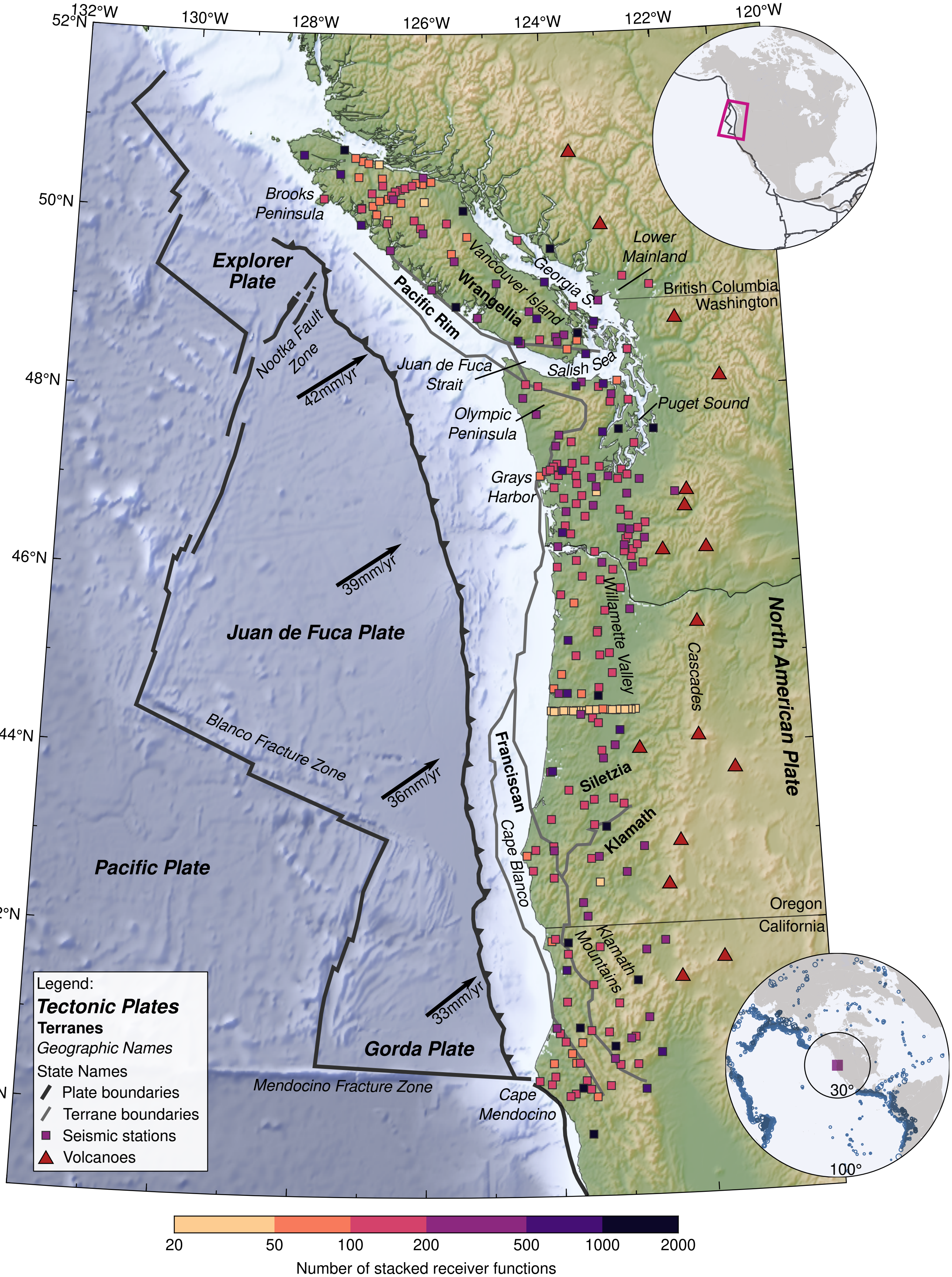
132°W
130°W
128°W
126°W
124°W
122°W
120°W
52°N
50°N
48°N
46°N
44°N
42°N
40°N
Brooks Peninsula
Explorer Plate
Nootka Fault Zone
42mm/yr
Pacific Rim
Wrangellia
Vancouver Island
Georgia S.
Lower Mainland
British Columbia
Washington
Juan de Fuca Strait
Salish Sea
Olympic Peninsula
Puget Sound
Grays Harbor
39mm/yr
Juan de Fuca Plate
Willamette Valley
Cascades
North American Plate
Blanco Fracture Zone
36mm/yr
Franciscan
Siletzia
Klamath
Cape Blanco
Pacific Plate
Oregon
California
Klamath Mountains
33mm/yr
Gorda Plate
Mendocino Fracture Zone
Cape Mendocino
30°
100°
Legend:
Tectonic Plates
Terranes
Geographic Names
State Names
Plate boundaries
Terrane boundaries
Seismic stations
Volcanoes
20
50
100
200
500
1000
2000
Number of stacked receiver functions

Figure 1. Tectonic setting of the Cascadia subduction zone and station distribution employed to determine the slab geometry under the forearc. Convergence of the Juan de Fuca and Gorda Plates relative to stable North America shown as arrows (**?**). Terrane boundaries modified after **?**. Top inset: Location of the study area on the North American continent. Bottom inset: Earthquake source distribution form 30° to 100° epicentral distance used to compute receiver functions.

oceanic crust is testament to complex deformation processes affecting slab morphology along the subduction trajectory.

2 Data and Methods

A total of 45,601 individual receiver functions recorded at 298 seismic stations distributed across the Cascadia forearc contributed to the slab model. For each station, 100 s recordings symmetric around the *P*-wave arrival of earthquakes with magnitudes between 5.5 and 8, in the distance range between 30 and 100°, were downloaded (Fig. 1). Waveforms with a signal-to-noise ratio smaller than 5 dB on the vertical component or 0 dB on the radial component were excluded. The instrument responses were removed and the seismograms were transformed to the upgoing *P*-*SH*-*SV* modes (**?**). The *P*-component was trimmed to the time window beyond which the envelope fell below 2% of the maximum amplitude and a cosine taper was applied. The three component *P*-wave spectra were scaled by their signal-to-noise ratio and binned according to their incidence angle in back-azimuth bins of 7.5° and horizontal slowness bins of 0.002 s km^{-1}. Within each bin, radial and transverse receiver functions were computed through frequency-domain simultaneous deconvolution (**?**), with an optimal damping factor found through generalized cross validation (**?**). This operation yielded the radial (R) and transverse (T) receiver functions.

The continental forearc and subducting slab were parameterized as three layers over a mantle half-space, with the subduction stratigraphy bounding interfaces labelled as t (top), c (central) and m (Moho) (Fig. 2). Synthetic receiver functions were calculated through ray-theoretical modeling of plane-wave scattering at the model interfaces (**??**, Fig. 2b). The thickness, S-wave velocity (V_S) and P- to S-wave velocity ratio (V_P/V_S) of each layer, as well as the common strike and dip of the bottom two layers and the top of the half space (in total 11 parameters) were optimized simultaneously through a simulated annealing global parameter search scheme (**?**), as implemented in the *SciPy* package (**?**). The misfit was defined as the anti-correlation (1 minus the cross correlation coefficient) between the observed and predicted receiver functions, bandpass filtered between 2 and 20 s period duration.

Initial thickness bounds for the continental crust (Fig. 2c) were based on the slab model of **?** (±10 km). Maximum Layer 1 thickness was constrained by the maximum E-layer thickness of 10 km (**?**), maximum Layer 2 thickness with the thickness of the incoming oceanic crust of 6.5 km (**?**). Layer 1 could attain zero-thickness if the E-layer were absent. Because the igneous oceanic crust may be part of the E-layer, Layers 1 and 2 were constrained to have a combined minimum thickness of 6 km. Velocity bounds (Fig. 2c) for the continental crust and Layer 2 were based on the 2σ interval of the expected lithologies for continental and oceanic crust, respectively, from the seismic velocity database of **?**; and for Layer 1 on an analytic poro-elastic model (**?**) constrained to match the V_P/V_S observations of the ULVZ (**?**).

The global search was initialized with at least three different random number seeds to verify convergence towards a global minimum. The resulting data predictions and mod-

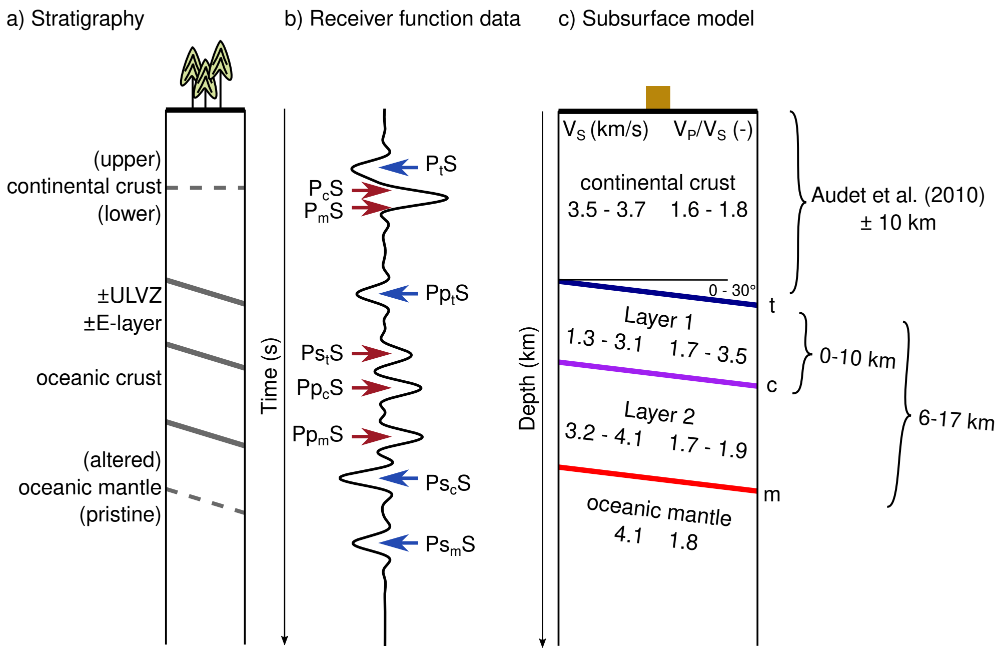

Figure 2. a) Forearc stratigraphy with the previously identified interfaces. b) Schematic radial receiver function with the forward and back scattered mode conversions used to constrain the model. Phases may interfere and cancel out in some cases. Absence of specific phase combinations may therefore be meaningful. Upper case letters indicate up-going rays, lower case letters down-going rays, subscript the scattering interface. c) Parameterization of the subsurface model. The possible presence of additional interfaces complicates the phase associations.

els were checked for consistency with neighboring stations, previous tomographic profiles (**????**), hypocentral locations of low-frequency earthquakes within tremor (**?????**) and offshore marine seismic profiles (Suzanne Carbotte, pers. comm; **?**). If none of the minimum misfit models of an individual station were consistent with the above constraints, the global search was repeated within narrower bounds around a preferred solution from a neighboring, reliable station. Such a model was only used in case it converged toward a value far from any thickness bound (Fig. 3). For each of the three horizons, a quality and a nominal depth uncertainty were assigned. Quality A denotes a horizon where at least one back-scattered phase in the predicted data correlates with the observed data (Fig. 3a and b), the predicted data are consistent among neighboring stations and the modeled horizon depth is consistent with the available external constraints. A quality B horizon shows a good phase correlation, but the predicted data are inconsistent with neighboring stations and/or the modeled depth is inconsistent with external constraints. A quality C was assigned to horizons that do not show a convincing correlation between observed and predicted data, usually due to data with low signal-to-noise levels. Stations above the forearc lowlands for which the characteristic slab signature (Fig. 2b) is decisively absent and where the onset of eclogitization is expected, were marked with a quality X. The nominal depth uncertainty was estimated from the scatter of the local minima in the vicinity of the preferred minimum as determined in the global search (Fig. 3c).

2.1 Fitting of interfaces

In total, 171, 143 and 137 quality A nodes were determined to constrain the t, c and m interfaces, respectively. At the trench, 105 nodes at 3 km below the local bathymetry

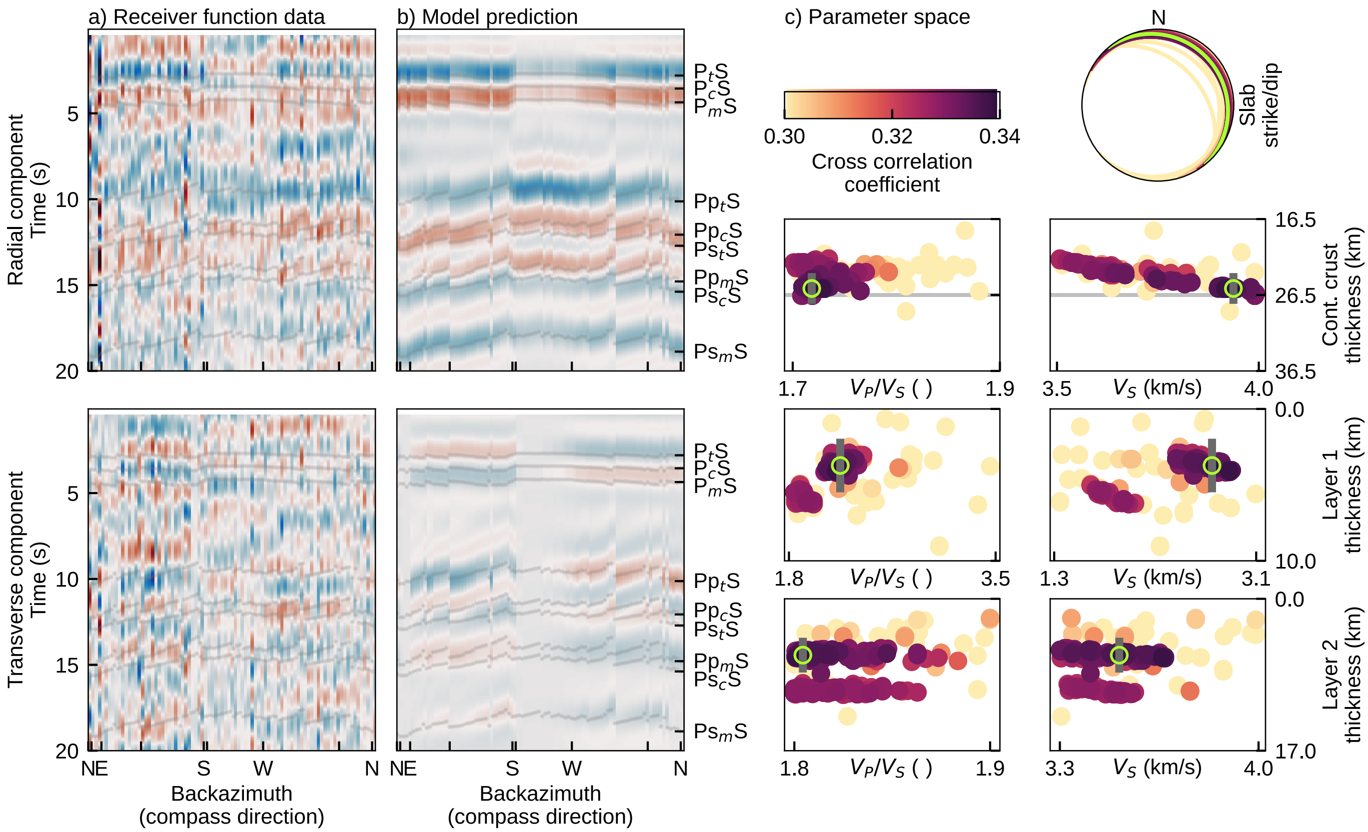

Figure 3. Global search for subsurface parameters. (a) Receiver function data for station C8.TWBB. (b) Predicted data from the best fitting model with phase labels as in Figure 3. (c) Local minima encountered in the global search for the 11 subsurface parameters using a simulated annealing scheme with preferred solution marked with a green circle and nominal depth uncertainties with a gray bar. Note the presence of a local minimum. If such minimum proved more consistent with external constraints and neighboring stations, the global search was repeated within bounds around that minimum.

were inserted to constrain the t and c interfaces, and at 6.5 km deeper to constrain the m interface, representing typical sediment and igneous crustal thicknesses (**?**). A spline surface (**?**) was fit to these nodes to yield margin-wide depth models. The spline coefficients were found using singular value decomposition, with the nominal depth uncertainties supplied as weights. The solution was damped using using the 116, 117, and 116 largest singular values for the t, c and m interfaces, respectively, based on analysis of L-curves and the Akaike information criterion (Fig. S1).

3 Results

3.1 Margin-scale slab morphology

The signature of subduction stratigraphy can be traced along the forearc from Brooks Peninsula on northern Vancouver Island, across Vancouver Island, Olympic Peninsula, the Willamette Valley of Washington and Oregon to Cape Mendocino and into Klamath

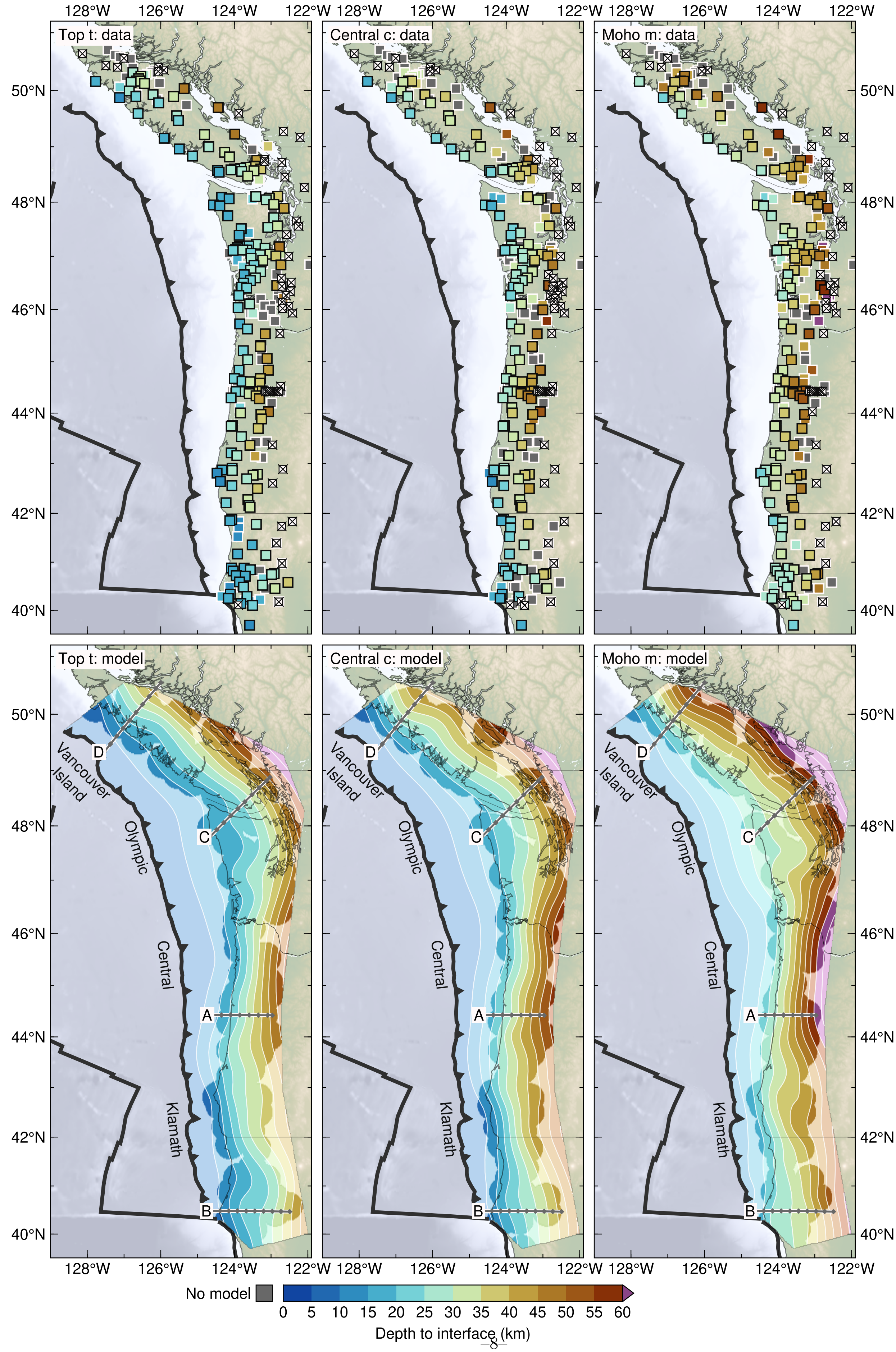
Top t: data
Central c: data
Moho m: data
Top t: model
Central c: model
Moho m: model
128°W
126°W
124°W
122°W
50°N
48°N
46°N
44°N
42°N
40°N
Vancouver Island
Olympic
Central
Klamath
A
B
C
D
No model
0
5
10
15
20
25
30
35
40
45
50
55
60
Depth to interface (km)

Figure 4. Depth to the t, c and m horizons. Top row: Data points by quality (black frames: A; white frames: B; not used for fitting the interface; grayed out: C). Stations marked X do not show the respective interface and are interpreted as the location of the eclogitization front. Bottom row: modeled interfaces and profile locations (Figs 5–8)

Mountains in northern California (Figs S2-S50). Recovered velocities of the three model layers are consistent for neighboring stations (Fig. S51). Slab morphology suggests a division into four segments: the Klamath, Central, Olympic and Vancouver Island segments (Fig. 4). The Central segment, between 44° N and 47° N, reveals the steepest dip, between 10 and 20°, and overall deepest slab, with the t horizon located between 15 and 25 km depth along the coast and dipping to 35 to 45 km depth before losing expression in advance of the volcanic arc. The Central segment is flanked to the north and south by flatter segments. In the south, the Klamath Segment, located between ∼40 °N and 44 °N, displays a more shallowly dipping slab, a contorted t horizon beneath Cape Mendocino and a contorted m horizon along the landward projection of the Blanco Fracture zone. The Olympic Segment, located between 47° N and 49° N, exhibits a shallow dipping (0-5°) slab beneath the coastal region, and is delimited to the south by steep downward bend in the t and m horizons near Gray's Harbour and by a bend in slab strike just north of the Juan de Fuca Strait. Along dip, the slab steepens as it approaches Puget Sound, where it begins to lose expression (**?**). The northernmost Vancouver Island segment is characterized by a moderately dipping slab. Near the northern terminus of subduction, north of Nootka Island, the t and c conversions appear disturbed. In summary, from north to south, the slab (i) dips gently and steepens down dip under Vancouver Island, (ii) dips shallowly beneath the Olympic Peninsula, (iii) steepens significantly beneath the Oregon Coastal Mountains, (iv) subducts in a step-like fashion in front of Klamath Mountains, and (v) becomes contorted in the Cape Mendocino area. A comparisson with previous slab models is shown inf Figure S52.

3.2 Regional scale

3.2.1 Central segment

Across the Central segment, the slab has been imaged with various seismological methods using data from the CASC'93 experiment (**????**). The comparison of our model with the teleseismic full-waveform tomogram of **?** yields a consistent picture of the subduction stratigraphy (Fig. 5). As in previous studies, **?** image the subducting Juan de Fuca plate as a distinctive low-V_S zone, which attains velocities as low as 3.3 km s^{-1}. All three horizons parallel this structure, with t marking the top of the LVZ and c and m marking two steps in the gradual increase towards high V_S, characteristic for oceanic mantle on the order of 4.3 km s^{-1}. This structure has a very clear and characteristic expression in the receiver functions, which weakens near station XZ.A18, beneath the Willamette Valley, as in the tomogram. The entire stratigraphic (t, c, m) sequence brackets weak slab-related seismicity in the offshore area (**?**). It has a thickness of about 7 km near the coast and thickens arc-ward to about 13 km, with the two layers possessing comparable thickness.

3.2.2 Klamath segment

Beneath the Mendocino region, the subduction stratigraphy has been imaged as a moderately high-V_P/V_S zone (1.8-1.9; **?**) complemented by relatively abundant intraslab seismicity defining tightly confined Wadati-Benioff zone (e.g., **??**, Fig. 6). The t and m horizons encapsulate the seismically active moderately high-V_P/V_S zone, with the m horizon falling in good agreement with the $V_P/V_S = 1.7$ contour. Where it projects

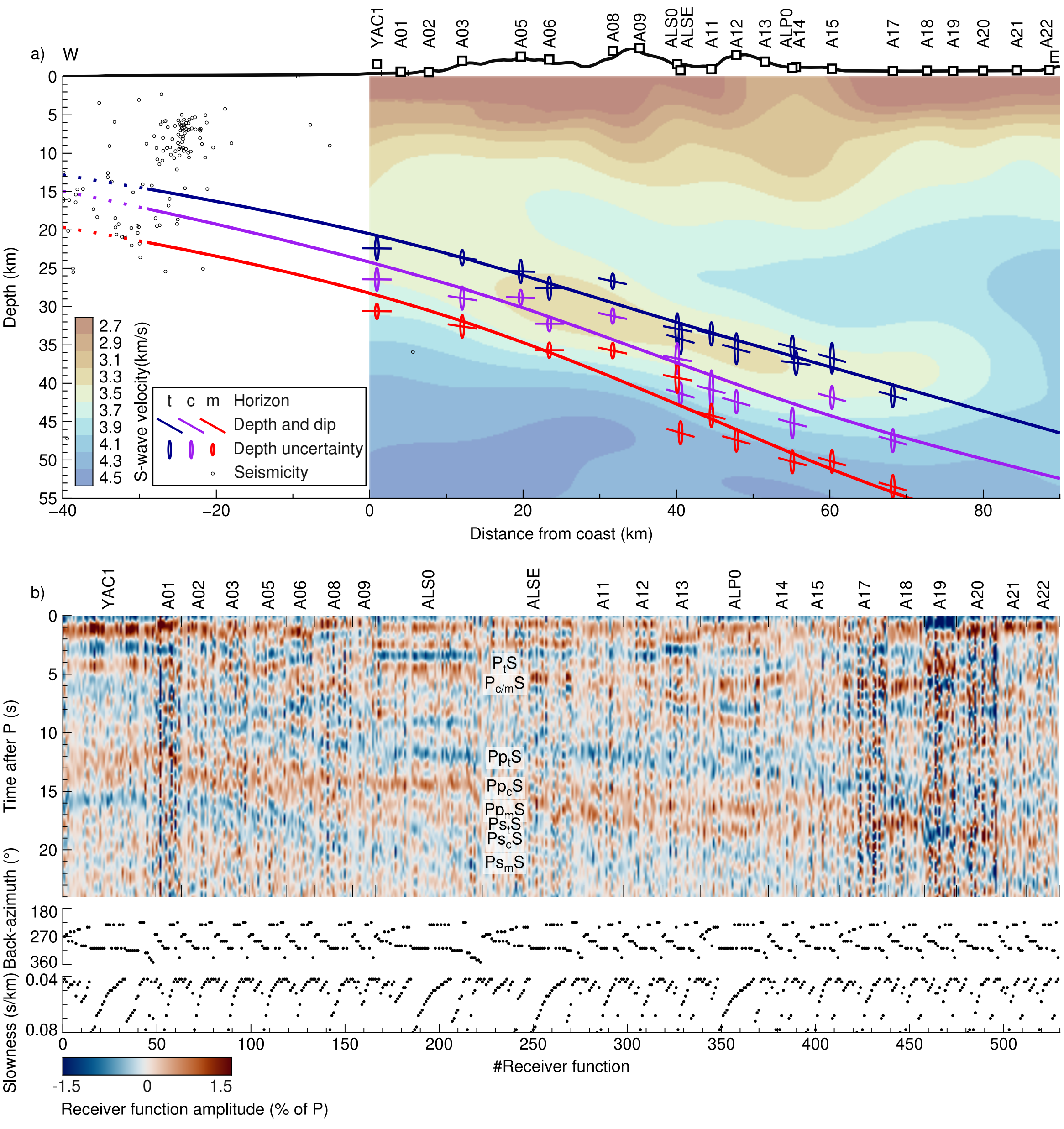

Figure 5. a) Profile A (Fig. 4) with slab model and control points superimposed on the V_S model of **?** with seismicity from **?**. Comparison with the V_P/V_S image is shown in Fig. S53. b) Receiver function sections of individual stations sorted along the profile, with receiver function within each section sorted by angular distance of the ray back-azimuth from profile azimuth (90°). 1.5–20 s bandpass filter applied. Phase labels correspond as in Fig. 2.

beneath the Franciscan terrane the high-V_P/V_S-zone loses expression and the density of earthquakes diminishes (60 km from coast in Fig. 6a). Our slab model here indicates a generally shallower dip that steepens again under the Klamath terrane (100 km from the coast), where our model indicates that a low-V_P/V_S anomaly is located within the subduction stratigraphy. Layer 1 is absent between the coast and the Franciscan terrane and attains a thickness of a few kilometers farther landward. Notably, no seismicity locates within Layer 1. The c horizon defining the base of Layer 1 approximately aligns with the location of LFEs (**?**). The entire subduction stratigraphy has a fairly uniform thickness of 10 km. The receiver function slab signature is difficult to correlate laterally, due presumably to some combination of variation in overburden and slab properties (Fig. 6b).

3.2.3 Olympic segment

A profile along dip from the western end of the Olympic Peninsula, over the Juan de Fuca Strait, southern Vancouver Island, and into the Strait of Georgia reveals a flat lying slab beneath Olympic Peninsula that advances under the Juan de Fuca Strait and gradually steepens under southern Vancouver Island (Fig. 7a). The t and m horizons encompass the moderately high-V_P/V_S zones previously interpreted as the subducting crust in local seismic tomograms (**??**). Under Olympic Peninsula, this zone is seismically active and m agrees well with the $V_P/V_S = 1.7$ contour. Beneath southern Vancouver Island, m bounds the top of seismic activity previously interpreted to occur within the subducting mantle (**?**). Layer 1 is absent or very thin beneath Olympic Peninsula and attains a thickness of about 5 km beneath southern Vancouver Island, where it is aseismic. The c horizon is located 2-3 km above a prominent band of LFE locations (**??**). Tremor hypocenters (**?**) scatter within and above the subduction stratigraphy. The complex overburden structure of Olympic peninsula hampers a clear identification of c and m; however, correlations of seismic phases along strike and along dip yield a laterally coherent picture. Beneath southern Vancouver Island, the slab reveals a clear and simple receiver function signature that can be traced beneath the Gulf Islands in the Strait of Georgia and loses expression toward the British Columbia Lower Mainland (Fig. 7b)

3.2.4 Vancouver Island segment

The Vancouver Island segment exhibits t and m horizons that bracket NE-dipping regions of elevated V_P/V_S evident in local seismic tomograms. The m horizon coincides with the $V_P/V_S = 1.7$ contour, that also bounds the top of seismicity which has been inferred to reside in the oceanic mantle (Figs. 8a and S3–S16; **??**). c can best be seen as a pronounced and distinct horizon in southern and south-central Vancouver Island, where it lies 2-4 km underneath t and decisively above LFE locations (**?**).

Towards north-central Vancouver Island, the subduction stratigraphy appears to thicken substantially downdip, from ∼8 km near the coast, to ∼16 km inland. Layer 1 and Layer 2 contribute in equal part to the combined thickness. The c horizon generally follows the LFE locations (**?**). Substantial scatter in the station measurements and difficulties in reconciling phase correlations across closely spaced stations attest to the complex subsurface structures that are also evident in local seismic tomography and may be related to subduction of the Nootka Fault Zone as the northern terminus of JdF subduction (Fig. 8b; **??**).

4 Interpretation of the subduction stratigraphy

The combined thickness of the stratigraphic package comprising t, c, m horizons almost everywhere exceeds the nominal thickness of the incoming oceanic crust of ∼6.5 km by 2 to 12 km (Fig. 9a). A thickness of ∼7 km is only resolved along the southern Central segment, between ∼43 and 44° N. Model regularization may dampen slab complex-

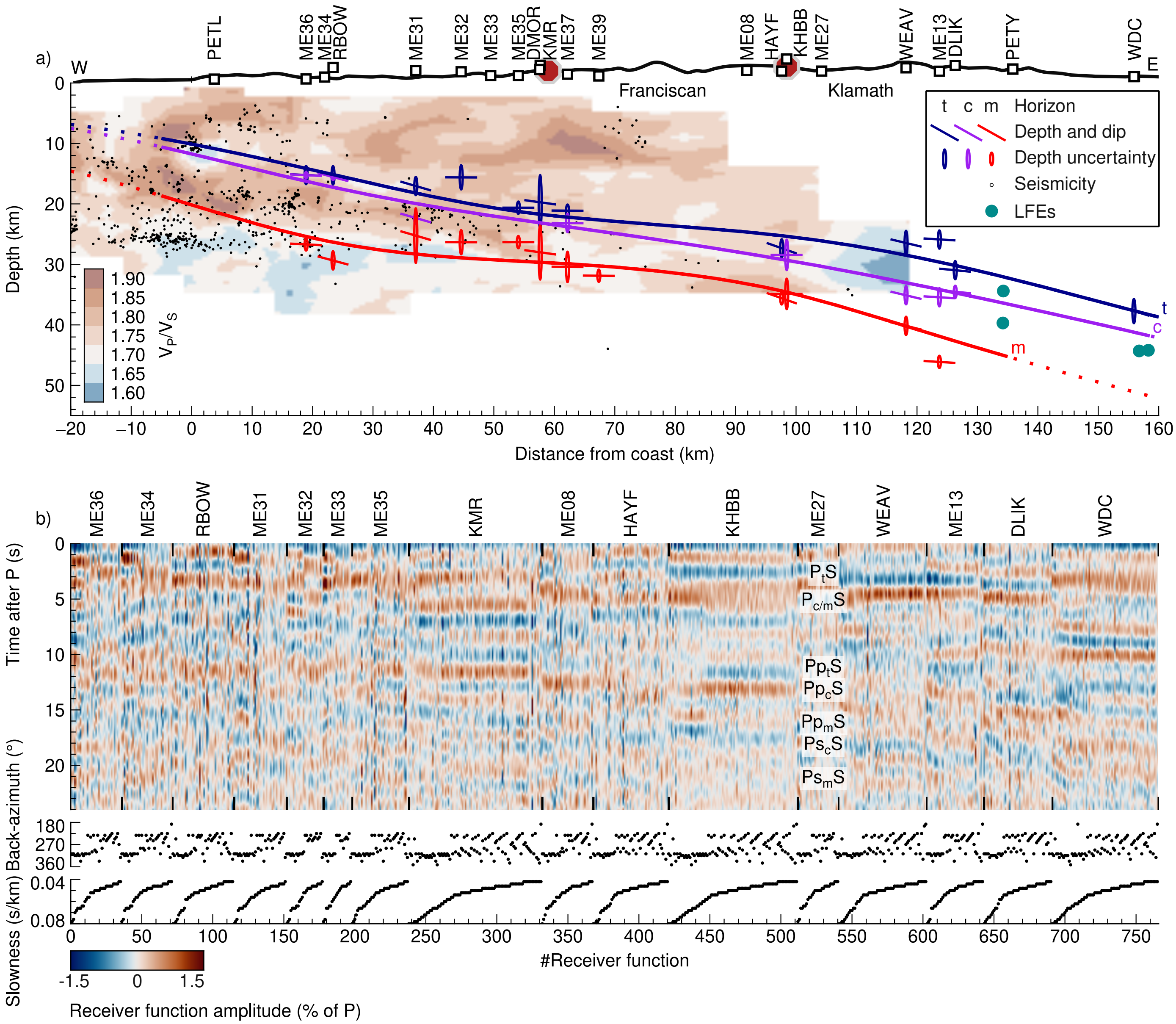

Figure 6. As Figure 5, but for Cape Mendocino profile B (see Fig. 4). Tomogram and seismicity from **?**, LFEs from **?**. A comparison with the V_S image is presented in Figure S54. Receiver functions filtered between 2 and 20 s.

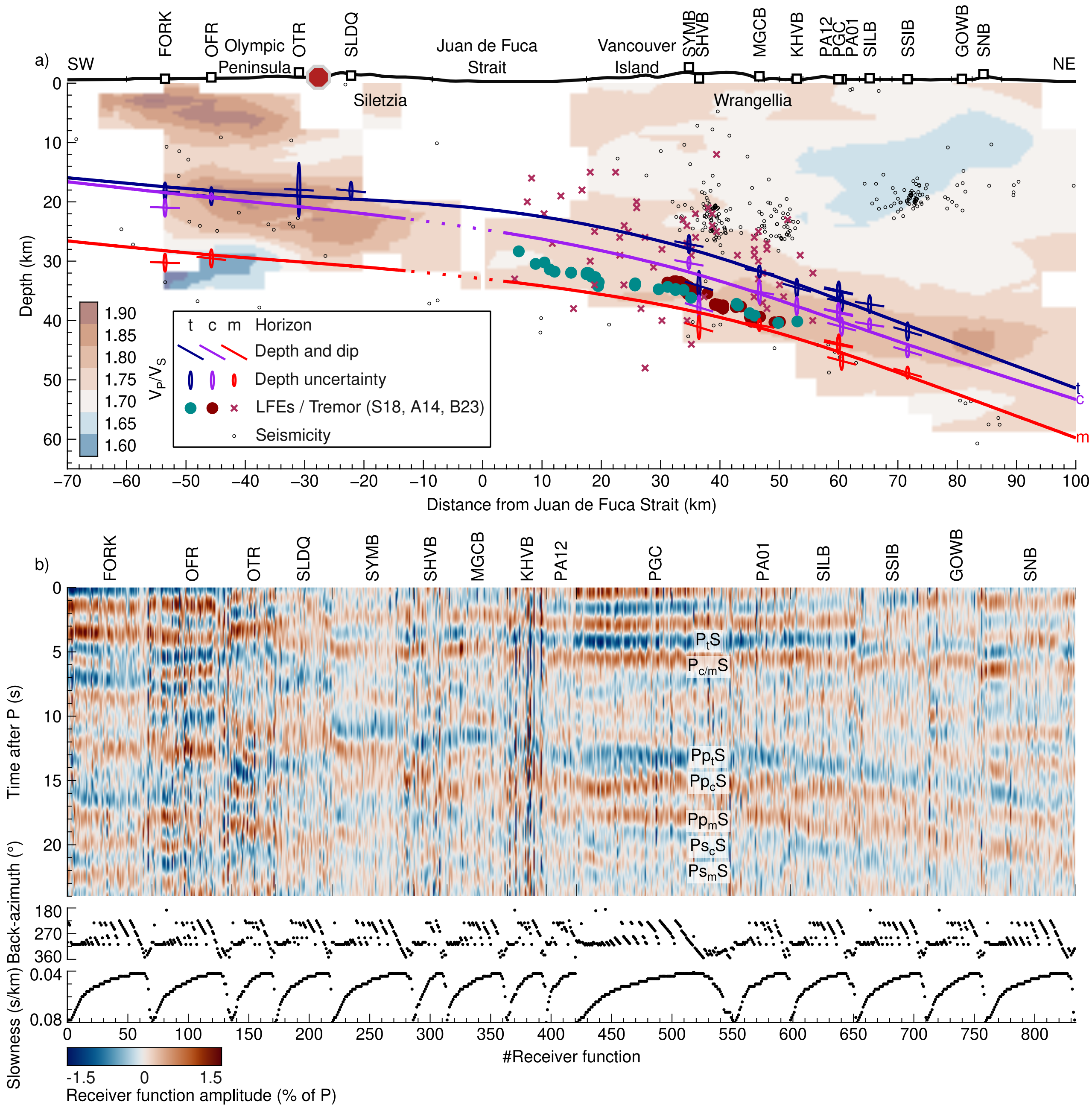

Figure 7. As Figure 5 for profile C across Olympic Peninsula (negative profile distances) and Southern Vancouver Island (positive profile distances). Tomograms and seismicity from **?** (Olympic Peninsula) and **?** (Vancouver Island). LFE and tremor locations are from: (A14) **?**; (S18) **?**; (B23) **?**. Comparisson with V_S shown in Figure S55. Receiver functions filtered between 2 and 20 s.

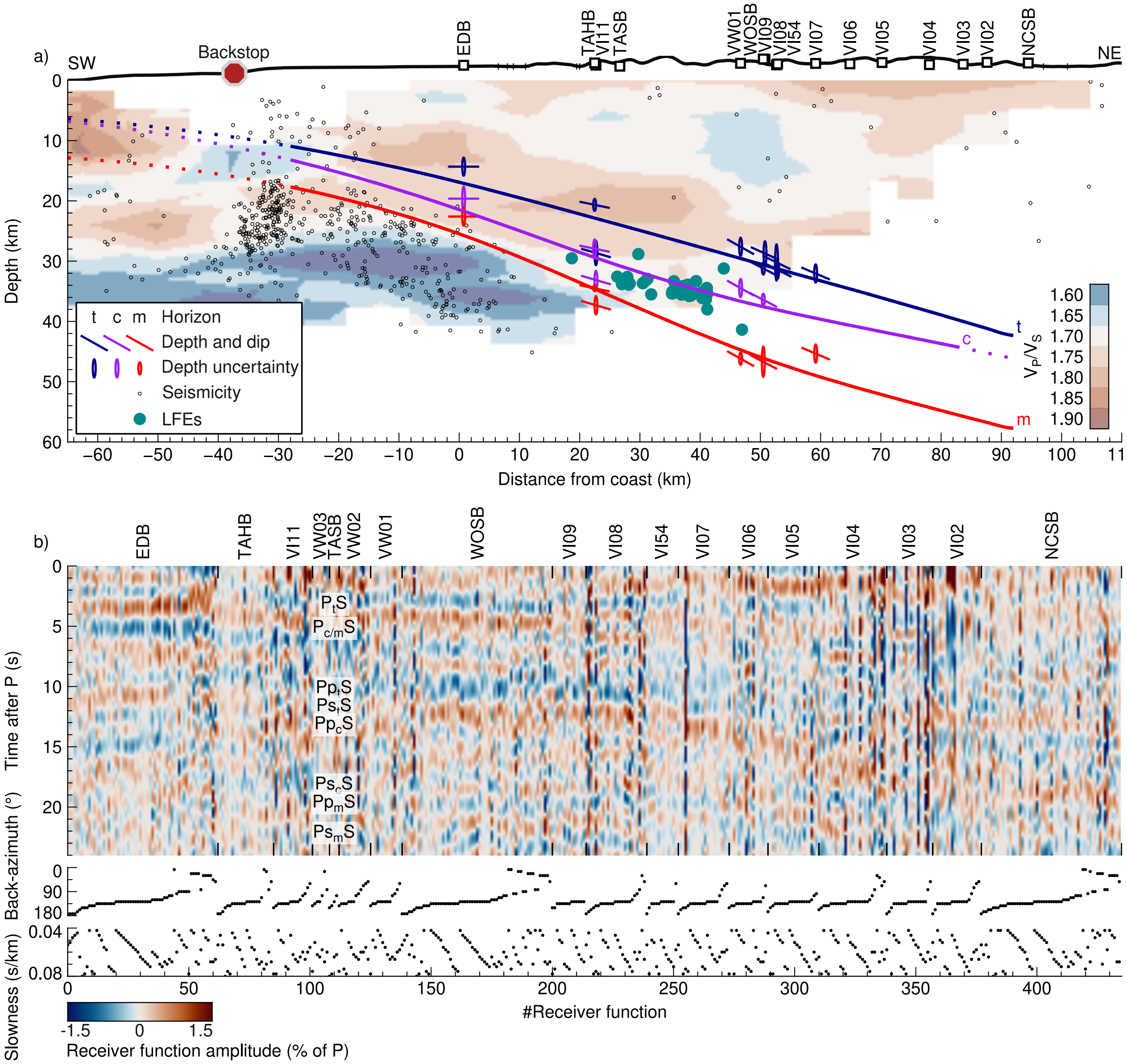

Figure 8. As Figure 5, but for profile D across Northern Vancouver Island. Tomogram and seismicity from **?**. LFE locations from **?**. Comparison with V_S shown in Figure S56. receiver functions filtered between 2 and 20 s.

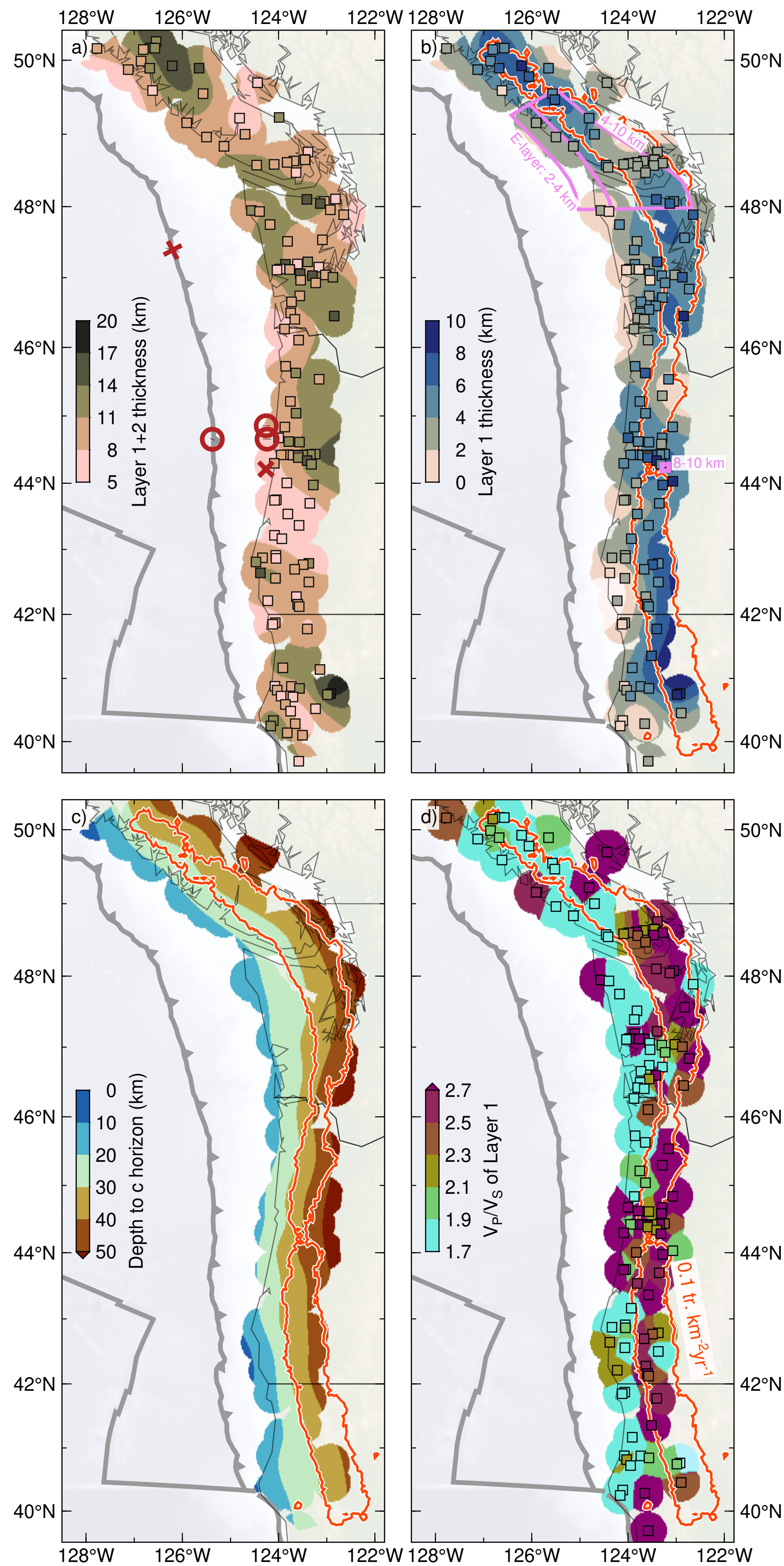

a)
b)
c)
d)
128°W
126°W
124°W
122°W
50°N
48°N
46°N
44°N
42°N
40°N
Layer 1+2 thickness (km)
20
17
14
11
8
5
Layer 1 thickness (km)
10
8
6
4
2
0
4-10 km
E-layer: 2-4 km
8-10 km
Depth to c horizon (km)
0
10
20
30
40
50
V_P/V_S of Layer 1
2.7
2.5
2.3
2.1
1.9
1.7
0.1 tr. km^{-2}yr^{-1}

Figure 9. Select properties of slab stratigraphy. a) Combined Layers 1 and 2 (t-to-m) thickness. 'O' marks places where sediment subduction has been detected on marine seismic surveys, 'X' where sediment subduction is absent (**??**). The thickness of the subduction stratigraphy exceeds the thickness of the igneous oceanic crust. b) Layer 1 (t-to-c) thickness and tremor zone (**?**). Downdip thickening of Layer 1 correlates with tremor locations. c) Depth to c horizon correlates closeley with tremor occurrence (Fig. 10c and d). d) V_P/V_S of Layer 1.

ity and smooth over interface steps on a ~20 km scale (e.g m in Fig. 6a), but the excessive thickness of the slab stratigraphy is a robust feature of the model and is almost always underpinned by individual point station measurements. Additional material, other than igneous oceanic crust, must therefore make up the subduction stratigraphy.

Layer 2 and the underlying mantle half-space, separated at m, were designed to correspond to igneous oceanic crust and pristine mantle. Where seismic velocities and seismicity images are available, the model appears to have captured this contrast appropriately, so that we confidently interpret m as the oceanic Moho. We cannot exclude the possibility that, where the plate is hydrated, m is biassed into the oceanic mantle, lying deeper than the Moho. Signs of mantle hydration may be present under the Cape Mendocino coast and offshore Northern Vancouver Island, suggested by a diffuse tomographic Moho, abundant mantle seismicity and the subduction of major fracture zones (Figs. 6 and 8, e.g., **????**). Such signatures are, however, not universally present.

The excess thickness is more likely developed above the locus of active the subduction, in Layer 1. Where the thickness of Layer 1 is substantial (i.e., from t to c; Fig. 9b), the E-layer (or a reflective zone above the slab) have been detected in reflection seismic surveys (Fig. 9b; **????**). **?** suggest that emergence of the E-layer is related to the occurrence of episodic tremor and slip. The E-layer is typically thicker than Layer 1, that is, Layer 1 is part of the E-layer. Within the tremor zone, defined as 0.1 tremor yr^{-1}km^{-2} (Fig. 9b-d; **?**), the mean and median V_P/V_S in Layer 1 are 2.49 ± 0.14 (2σ) and 2.44. Outside the tremor zone V_P/V_S is lower, with a mean value of 2.28 ± 0.14 and median value of 1.95 (Figs. 9b, 10a and b). A two-sample Kolmogorov-Smirnov test yields a p-value of $5{\cdot}10^{-5}$, indicating that the Layer 1 V_P/V_S values inside and outside the tremor zone are not drawn from the same population, suggesting that the development of Layer 1 as a high-V_P/V_S ULVZ is related to tremor, in agreement with previous findings (**??**). We interpret t in the tremor zone as the top of this ULVZ. Projecting the tremor epicenters (**?**) onto the t and c horizons yields tremor depth of 32 ± 10.8 km and 38 ± 10.2 km (2σ), respectively (Fig. 10c and d). Tremor depth are concentrated more tightly when projected to the c horizon, suggesting tremor occurs closer to the base of Layer 1 (Fig. 9c). Inside the tremor zone, where Layer 1 corresponds to the ULVZ, c marks a stark material contrast against the underlying oceanic crust and we interpret c as the base of the ULVZ.

Between the coast and the tremor zone, except between 44 and 45° N, Layer 1 is typically thinner (Fig. 9b) and its V_P/V_S is lower (Figs. 9d and 10b), attaining normal values for basaltic material (~1.8). Layers 1 and 2 still exhibit a combined thickness in excess of the incoming oceanic crust with Layer 1 displaying properties that are, nevertheless, similar to oceanic crust. The t horizon is here the top of this excess volume. The c horizon here usually marks a less prominent material contrast than inside the tremor zone. It may seem natural to interpret c as the base of a possible sedimentary blanket above an underlying igneous oceanic crust (e.g., **?**), but we note here that Layer 2 is frequently thicker than oceanic crust, hence the interpretation of c as the base of sediments is possible, but not universal. Horizon c may alternatively represent a velocity gradient

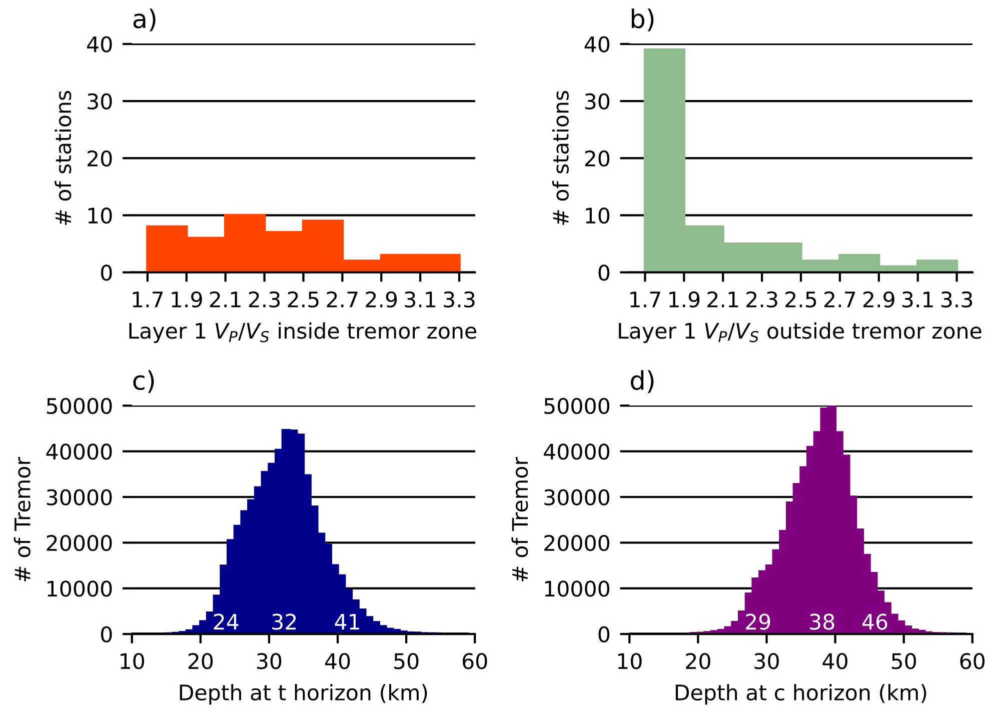

Figure 10. Properties of Layer 1 in relation to tremor. (a and b) V_P/V_S of Layer 1 at stations (a) inside and (b) outside the tremor zone (0.1 tremor km^{-2}yr^{-1} contour; Fig. 9). (c and d) Depth distribution of tremor epicenters projected onto the (c) t and (d) c horizons. Numbers at the base indicate the 5%, 50% and 95% quantiles of the depth distribution.

within a sedimentary layer or the base of altered material belonging to overriding continental crust.

5 Discussion

5.1 Control of slab morphology

The overall slab morphology exhibits a first-order correlation with the location of the crystalline accreted terranes that form static backstops in the Cascadia subduction system (Fig. 11; **?**). Most notably, where the Siletz terrane recedes far inland on the eastern side of Olympic Peninsula, giving way to the Olympic complex formed by underthrust marine sediments (e.g., **?**), the slab lies shallower and flatter than anywhere else along the entire onshore forearc. Conversely, where the western boundary of the Siletz terrane is located off-shore, the slab deepens and steepens significantly. It reaches its steepest dip where aeromagnetic and magneto-telluric measurements indicate that the Siletz terrane is most voluminous (**??**) and interseismic vertical uplift is lowest (**?**). This suggests that the competence and rigidity of the Siletz block forces the descent of the Juan de Fuca slab. It has been suggested that the Kumano pluton influences the subducting Philippine Sea Plate in a similar manner below southwest Japan (**?**).

In between the flat-lying Olympic and steeply dipping Central segments, a pronounced southward downward bend in the slab is evident along a line extending between Gray's Harbour and the southern end of Puget Sound. The bend is evident in the raw receiver

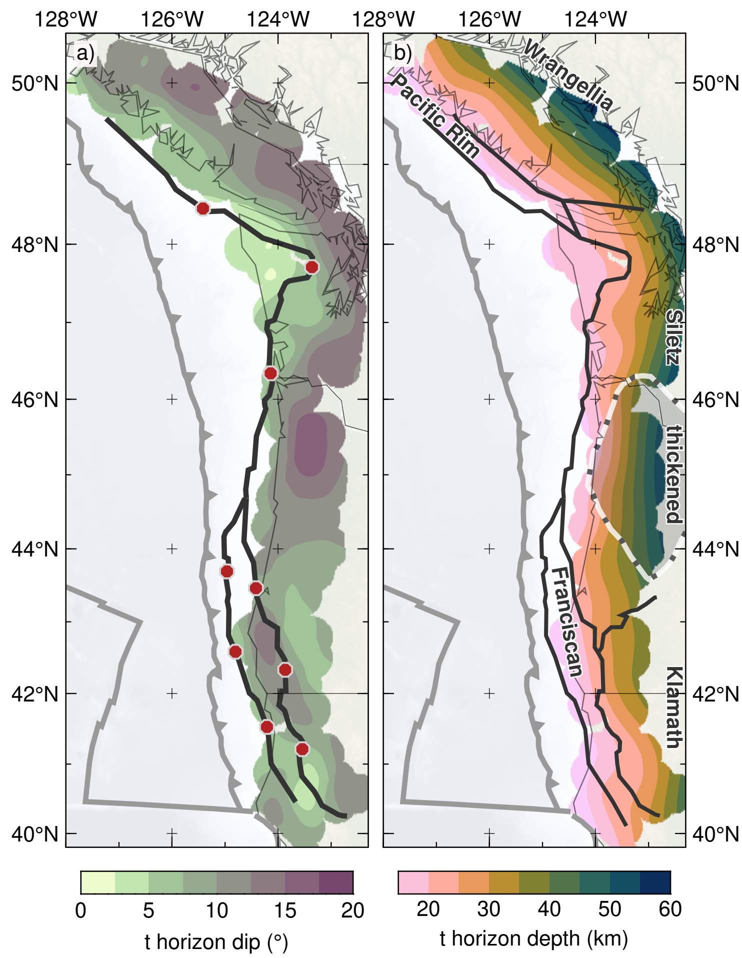

Figure 11. Dip (a) and depth (b) of the t horizon. Static backstop (line with red octagons in a) and terrane boundaries (thick lines in b) modified after **?**. Shaded area enclosed by white dashed line represents thickened Siletz terrane detected in aeromagnetic data (after **?**). The location of the terrane backstop correlates with and may exert a first order control on slab morphology.

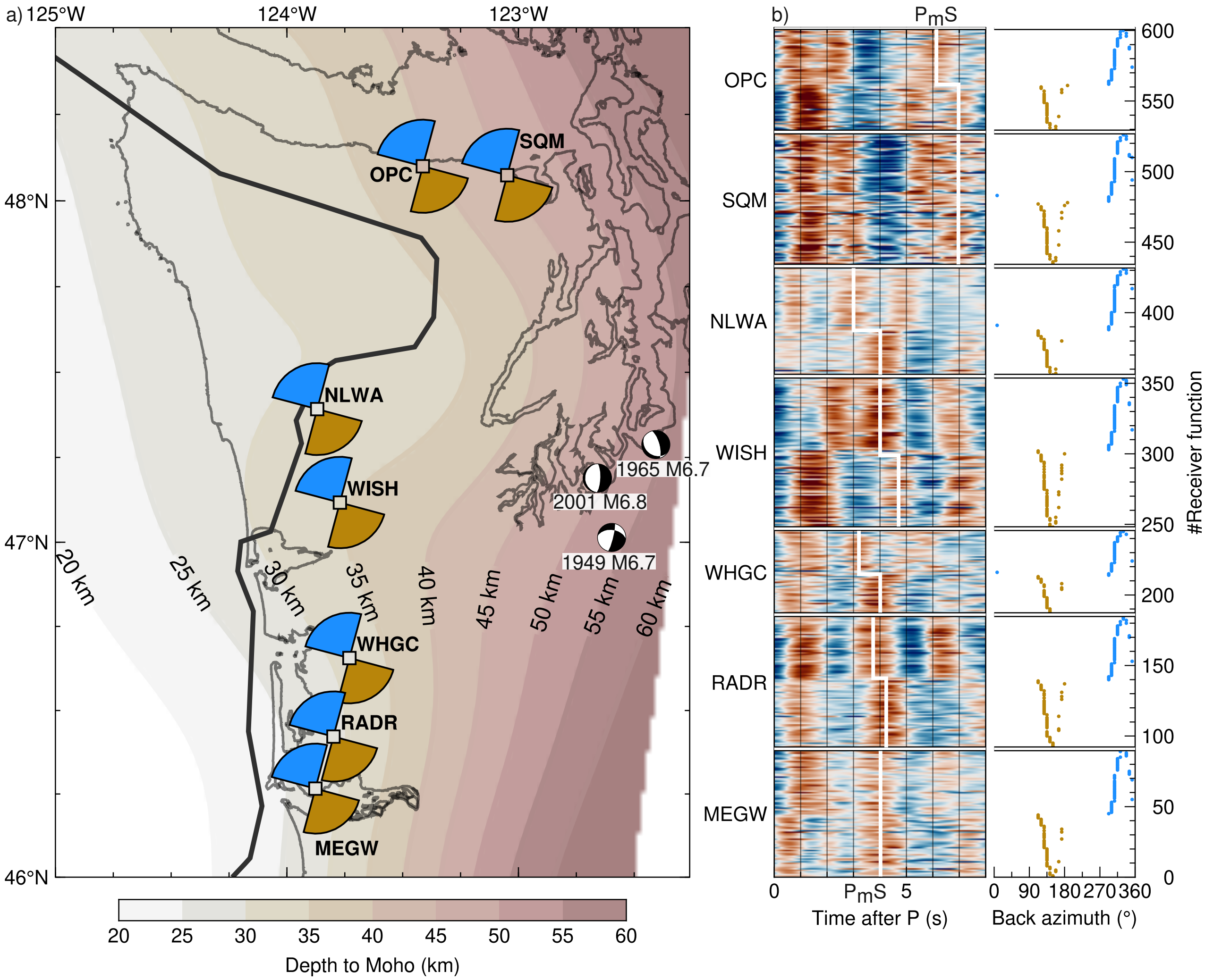

Figure 12. Downwarped Moho from Olympic Peninsula to Gray's Harbour. (a) Map view with Moho depth contours as well as locations and receiver function ray back-azimuths of stations shown on the right. Earthquake locations and focal mechanisms from **?**. (b) Receiver functions sorted by back-azimuth. Rays arriving from NNW colored blue, from SSW coloured gold. Note the southward down Moho-steps (P_mS) at stations coincident with a thickening low velocity zone above at stations NLWA, WISH, WHGC and RADR.

functions, where the timing of the P_mS conversion decreases, e.g., from ∼3 to ∼4 s for rays arriving from NNW relative to those arriving from SSE azimuths at station US.NLWA and again from 4 s to 4.5 s just south of that at station UW.WISH (Fig. 12). Perhaps significantly, the three largest intermediate depth earthquakes in Cascadia, the 1949 $M6.7$ Olympia (**?**), 1965 $M6.7$ Puget Sound (**?**) and 2001 $M6.8$ (**??**) earthquakes occurred near the down-dip continuation of this bend, at depths at or immediately below those projected for the oceanic Moho.

Along the Klamath segment to the south (south of 44°N), slab structure is complex. The Gorda Plate, a relatively young and highly deformed plate (**??**), encounters two static backstops, the Coastal Belt Fault and the western boundary of the Klamath terrane (Fig. 11; **??**), and the southern terminus of subduction at Cape Mendocino. The southern and eastward trending seaward boundary of the thickened Siletz terrane has a reduced impact on slab morphology, resulting in the southward transition to a more gently dipping slab (Fig. 11). This geometry is interrupted with emergence of the Klamath terrane, where the steepest dip of the slab is located near the coast, bending behind the first, seaward backstop, and unbending beneath the second, landward, backstop. In the Cape Mendocino area the slab top is contorted in a fashion that yields a flat-lying segment just behind the coast. Because of the generally lower dip in advance of the volcanic arc and its unbending beneath the southern Siletz and Klamath terranes, it appears as if the Gorda plate does not subduct as readily as the Juan de Fuca plate. A possible cause for this behaviour is an increased buoyancy of the youngest subducting lithosphere (5-6 Ma at the trench, e.g., **?**)

5.2 Excess thickness of Subduction Stratigraphy

The nature and origin of the E-layer as a prominent element of the subduction zone stratigraphy that emerges abruptly along the dip trajectory in the vicinity of southern Vancouver Island is a long standing conundrum in the understanding of the Cascadia subduction zone (e.g., **?????**). Our data show a qualitative correlation between a thick Layer 1 and a thick (>4 km) E-layer where the latter has been imaged (Fig. 9b). We also suggest that the reflective zone mapped by COCORP in central Oregon (Fig. 9b; **?**) may manifest the presence of a structure with similar origin since it also coincides with a thick Layer 1. Assuming this association holds true along the entire margin, our data would suggest that the E-layer is ubiquitous. Its abrupt emergence along dip is likewise reflected in our data: Coastal stations have a tendency to exhibit a thin or absent Layer 1, whereas inland stations generally possess a thick one (Fig. 9b), consistent with previous inferences of Layer 1 thickening near the coast line from an amphibious receiver function study (**?**). Interestingly, the combined (Layer 1 + Layer 2) thickness of the subduction stratigraphy does not obey the same trend. Places of a thin or absent Layer 1 may have an overall thick subduction stratigraphy (e.g., coastal Olympic Peninsula and Cape Mendocino) and a significantly thick Layer 1 may correspond to a subduction stratigraphy that does not much exceed the thickness of the incoming oceanic crust (e.g., $\sim$7 km thickness between 43° N and 44° N; Fig. 13a).

Sediments entering the subduction system may contribute to the subduction stratigraphy (e.g., **?**) but information about the amount of subducting sediment at the time of writing is scarce. **?** interpret sediments subducting beneath Siletzia on two seismic lines near 45° N (circles on Fig. 9a), but not on a third line closer to 44° N, (cross on Fig. 9a). Within the same latitude interval, the characteristic transition from thickened to normal subduction stratigraphy occurs, suggesting that these subducting sediments make up for the extra thickness (Fig. 13b). In contrast, **?** document no sediment subduction at the latitude of the Juan de Fuca Strait, where we image a thick ($\sim$11 km) subduction stratigraphy. However, it is possible that sediment subduction was occurring at the trench in the latter region at 3 Ma ago, and subsequently ceased. More data are required to define conclusively where sediment subduction contributes to subduction stratigraphy thickness.

We note that Layer 1 emerges at around 30 km depth and gains thickness along the subduction trajectory, and that this thickness is unrelated to the thickness of the subduction stratigraphy updip of this depth (Figs 9a and b). This observation suggests that Layer 1 thickens in-situ and develops a ULVZ through some depth-activated process. Elevated V_P/V_S (Figs 9b and d) suggests that the medium is fractured and saturated with pressurized fluids (**?**), implying it has lost structural integrity and strength. As a weak zone the ULVZ is likely to host slip. LFE hypocenters are located near the base of the ULVZ (Fig. 14; **?**), suggesting that the plate boundary is located near c. Excess thickness may be due to underplating of subducting material, either of sediments atop the oceanic crust (e.g., **?**), or of the upper basaltic crust which may lose structural integrity

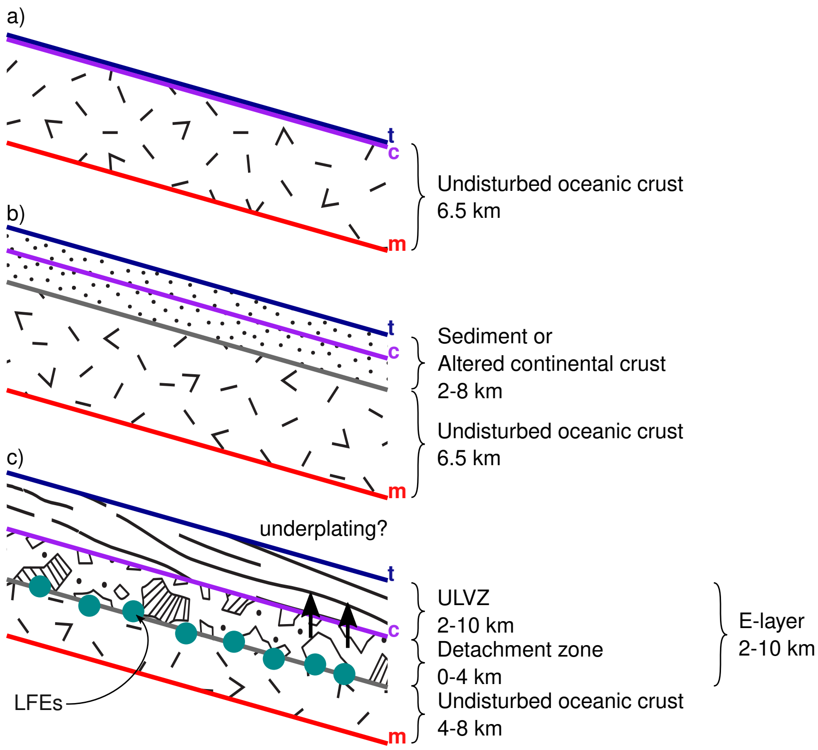

Figure 13. Possible subduction stratigraphies present in the Cascadia subduction zone. (a) Subduction of undisturbed oceanic crust (e.g. Central – South Oregon). (b) Sediment subduction, *c* may represent the base of the sedimentary later or a horizon within the sediments (e.g. Olympic Peninsula, Northern Oregon). (c) E-layer on top of the subducting crust. LFEs locations may indicate a detachment horizon at or below the base of the ULVZ. Low seismic velocities and in-situ thickening above suggest ongoing underplating (e.g. Southern Vancouver Island)

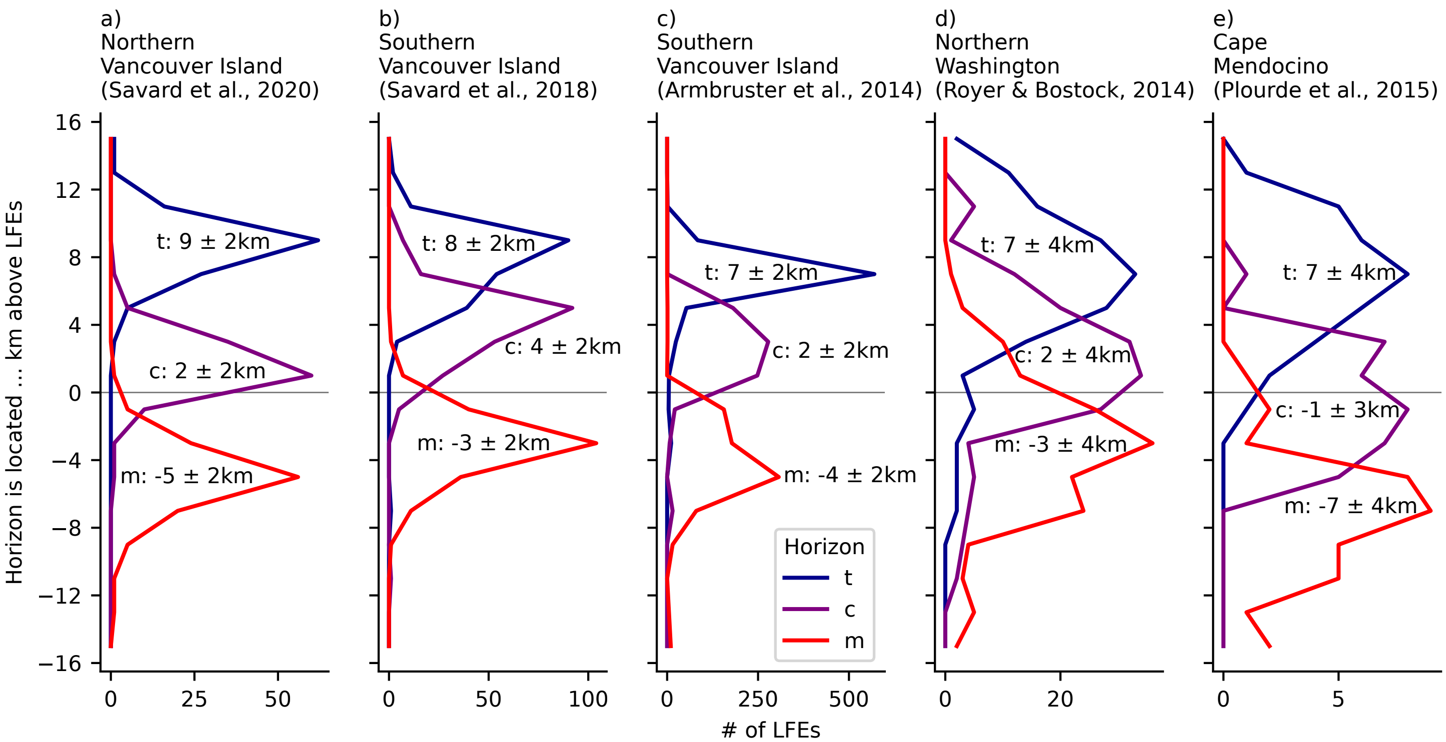

Figure 14. Histograms of the depth of t, c and m horizons relative to LFE locations for different regions. Bin width is 2 km. LFEs are most closely located to the c horizon. For Vancouver Island, the data indicate that LFEs occur in Layer 2, between c and m

through wear (Fig. 13c). Moderately high seismic velocities ($V_S > 3.2$ and $V_P/V_S < 1.9$) indicated by our inverse modeling results for Layer 2 (Figs. 2 and S51) preclude the presence of pervasive fracturing and pressurized fluids (?). Instead, the presence of slivers of oceanic crust, large enough to *not* reduce seismic velocities significantly, would be consistent with LFE occurrence inside Layer 2. The subordinate slip represented by the LFEs during ETS episodes is consistent with the process of initiating detachment of the subducting oceanic crust at the LFE horizon (Fig. 13c). Slow slip, which makes up the main share of the slip budget at depth (????), may well be located at or above c, that is at the base or inside the 4-10 km thick ULVZ.

Subcretion and underplating is consistent with earlier inferences made for the onshore Cascadia forearc from a wealth of geophysical data. ? interpret underplating as taking place south of Puget Sound. ? and ? inferred that the E-layer constitutes underplated material. The correspondence between these inferred sites of underplating with the thick ULVZ detected here and the widespread distribution of the ULVZ suggest that underplating is occurring through the majority of the entire Cascadia forearc (e.g., ?).

6 Conclusion

Receiver functions provide valuable insights into the subduction of the Juan de Fuca and Gorda plates in the Cascadia region. Based on previous studies of receiver-side forward and back-scattered mode conversions, we parameterize subduction stratigraphy in three horizons t, c and m. Mapping these horizons across the forearc reveals flatter slab segments beneath the Olympic Peninsula and Cape Mendocino, central Oregon exhibits a steeply dipping slab. Below most of Vancouver Island the slab is marked by modest dips. This slab morphology appears to be influenced by the strength and density of accreted crystalline terranes. A notable Moho step south of the Olympic Peninsula may relate to recurrent, large, intermediate-depth earthquakes beneath Puget Sound. In addition, the presence of a thick topmost layer in the subduction stratigraphy may indicate the widespread occurrence of the E-layer. Previous interpretations suggest that the E-layer represents underplated slab material, implying that underplating occurs through most of the Cascadia forearc.

Data and Code availability

The raw model parameters and slab horizons are part of the supplement of this manuscript and will be made available as a data publication after peer review. The networks with the following FDSN network coded were used in this study: BK (?), C8, CC (?), CN (?), IU (?), NC (?), PO, TA (?), UO (?), US (?), UW (?), X4 (2016-2021 ?), XA (2008–2009 ?), XD (2014–2016 ?), XQ (2007–2009 ?), XU (2006–2012 ?), XZ (1993–1994), YS (2001–2003 ?), YW (2007–2010 ?). Seismic waveforms are available via the IRIS Data Management Center (IRISDMC; `http://service.iris.edu/fdsnws/dataselect/1/`) and/or the Northern California Earthquake Data Center (https://service.ncedc.org/fdsnws/dataselect/1/). Receiver functions were processed with *RfPy* (?). Synthetic receiver functions were computed with *PyRaysum* (?). Numerical methods of the global parameter search are from *SciPy* (?), for signal processing and data manipulation from *NumPy* (?). Fitting of the spline surface was done with *greenspline*, which is part of *GenericMappingTools* (?). Maps were drawn with *PyGMT* (?). Graphs were plotted with *Matplotlib* (?). Seismic data were handled with *ObsPy* (?).

Acknowledgments

We thank Suzanne Carbotte for generous and substantive discussion and preview of CASIE'21 results. Hao Guo, Jeffrey McGuire, Leo Kan, Sebastien Chevrot, Reid Merrill and Genevieve Savard kindly made their seismic tomograms and relocated seismicity available. Paul Wessel and the *GMT* community supported the computation of regularized spline surfaces. Discussions with Raul Mendoza and Simon Peacock provided valuable insights into Cascadia forearc architecture. Funded by Deutsche Forschungsgemeinschaft grant BL 1758/1-1.

This research regards the ancestral homelands and waters of hundreds of diverse and distinct Indigenous Peoples. Among them are the Kwakwaka'wakw Peoples, the Nuu-chah-nulth Peoples, the Makah Peoples, the Coast Salish Peoples, the Quileute Peoples, the Chinookan Peoples, the Siletz People, the Cow Creek Band, the Grand Ronde Community, the Coos, Lower Umpqua, and Siuslaw Peoples, the Klamath Tribes, the Hupa People, the Yurok People, and the Karuk People. It was undertaken at the UBC Vancouver campus on the traditional, ancestral, and unceded territories of the Musqueam People and at the University of Ottawa, located on unceded Algonquin territory. Kayla Lar-Son of UBC's X̲wi7x̲wa Library provided assistance in the formulation of this land acknowledgment.